

Dynamical Systems and Their Bifurcations

Fabio Dercole¹ and Sergio Rinaldi^{1,2}

¹DEI, Politecnico di Milano
Via Ponzio 34/5, 20133 Milano, Italy
fabio.dercole[sergio.rinaldi]@polimi.it

²Evolution and Ecology Program, International Institute for Applied Systems Analysis
2361 Laxenburg, Austria

Summary

In this chapter we summarize the basic definitions and tools of analysis of dynamical systems, with particular emphasis on the asymptotic behavior of continuous-time autonomous systems. In particular, the possible structural changes of the asymptotic behavior of the system under parameter variation, called bifurcations, are presented together with their analytical characterization and hints on their numerical analysis. The literature on dynamical systems is huge and we do not attempt to survey it here. Most of the results on bifurcations of continuous-time systems are due to Andronov and Leontovich [see Andronov *et al.*, 1973]. More recent expositions can be found in Guckenheimer & Holmes [1997] and Kuznetsov [2004], while less formal but didactically very effective treatments, rich in interesting examples and applications, are given in Strogatz [1994] and Alligood *et al.* [1996]. Numerical aspects are well described in Allgower & Georg [1990] and in the fundamental papers by Keller [1977] and Doedel *et al.* [1991a,b], but see also Beyn *et al.* [2002] and Kuznetsov [2004]. This chapter mainly combines material from two previous contributions of the authors, the first part of the book *Biosystems and Complexity* [Rinaldi, 1993, in Italian] and the Appendix A of a recent book on evolutionary dynamics [Dercole & Rinaldi, 2008].

1 Dynamical Systems and State Portraits

The dynamical systems considered in this chapter are *continuous-time, finite-dimensional* dynamical systems described by n *autonomous* (i.e., time-independent) ordinary differential equations (ODEs) called *state equations*, i.e.,

$$\begin{aligned}\dot{x}_1(t) &= f_1(x_1(t), x_2(t), \dots, x_n(t)), \\ \dot{x}_2(t) &= f_2(x_1(t), x_2(t), \dots, x_n(t)), \\ &\vdots \\ \dot{x}_n(t) &= f_n(x_1(t), x_2(t), \dots, x_n(t)),\end{aligned}$$

where $x_i(t) \in \mathbf{R}$, $i = 1, 2, \dots, n$, is the i th *state variable* at time $t \in \mathbf{R}$, $\dot{x}_i(t)$ is its time derivative, and functions f_1, \dots, f_n are assumed to be smooth.

In vector form, the state equations are

$$\dot{x}(t) = f(x(t)), \tag{1}$$

where x and \dot{x} are n -dimensional vectors (the *state vector* and its time derivative) and $f = [f_1, \dots, f_n]^T$ (the T superscript denotes transposition).

Given the initial state $x(0)$, the state equations uniquely define a *trajectory* of the system, i.e., the state vector $x(t)$ for all $t \geq 0$. A trajectory is represented in state space by a curve starting from point $x(0)$, and vector $\dot{x}(t)$ is tangent to the curve at point $x(t)$. Trajectories can be easily obtained numerically through simulation (numerical integration) and the set of all trajectories (one for any $x(0)$) is called the *state portrait*. If $n = 2$ (*second-order* or *planar* systems) the state portrait is often represented by drawing a sort of qualitative skeleton, i.e., strategic trajectories (or finite segments of them), from which all other trajectories can be intuitively inferred. For example, in Figure 1A the skeleton is composed of 13 trajectories: three of them (A, B, C) are just points (corresponding to constant solutions of (1)) and are called *equilibria*, while one (γ) is a closed trajectory (corresponding to a periodic solution of (1)) called a *limit cycle*. The other trajectories allow one to conclude that A is a *repellor* (no trajectory starting close to A tends or remains close to A), B is a *saddle* (almost all trajectories starting close to B go away from B , but two trajectories

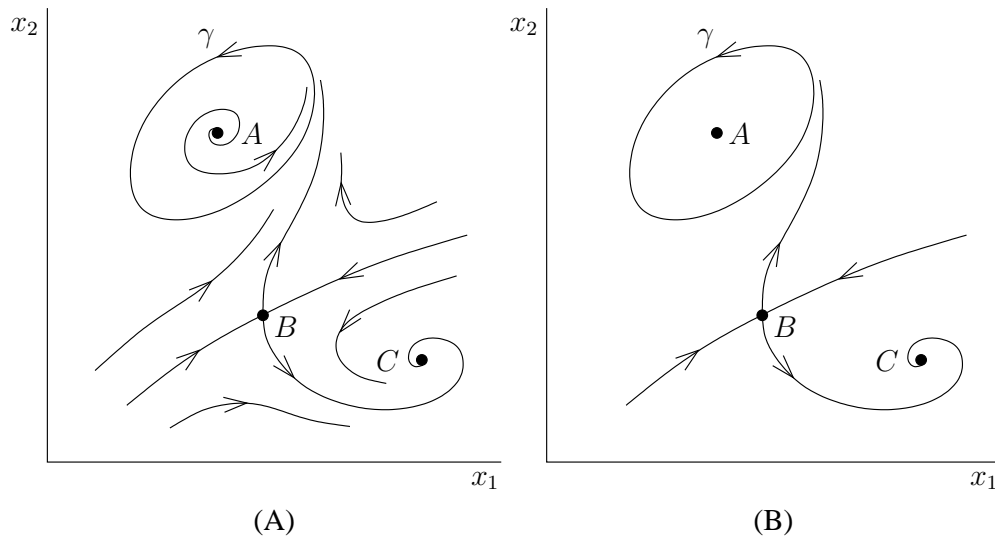


Figure 1: Skeleton of the state portrait of a second-order system: (A) skeleton with 13 trajectories; (B) reduced skeleton (characteristic frame) with 8 trajectories (attractors, repellers, and saddles with stable and unstable manifolds).

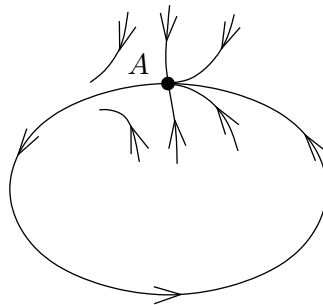


Figure 2: An example of unstable attractor: the equilibrium A .

tend to B and compose the so-called *stable manifold*; the two trajectories emanating from B compose the *unstable manifold* and both manifolds are also called *saddle separatrices*), while C and γ are *attractors* (all trajectories starting close to C [γ] tend to C [γ]). Attractors are said to be (*asymptotically*) *stable* if all nearby trajectories remain close to them, *globally stable* if they attract all initial conditions (technically with the exclusion of sets with no measure in state space), while saddles and repellers are *unstable*. Notice, however, that attractors can also be unstable, as shown in Figure 2, where the equilibrium A attracts all nearby initial conditions, part of which along trajectories going away from it.

The skeleton of Figure 1A also identifies the *basin of attraction* of each attractor: in fact, all trajectories starting above [below] the stable manifold of the saddle tend toward the limit cycle γ [the equilibrium C]. Notice that the basins of attraction are open sets since their boundaries are the saddle and its stable manifold.

Often, the full state portrait can be more easily imagined when the skeleton is reduced, as in Figure 1B, to its basic elements, namely attractors, repellers, and saddles with their stable and unstable manifolds. From now on, the reduced skeleton is called the *characteristic frame*.

The asymptotic behaviors of continuous-time second-order systems are quite simple, because in the case $n = 2$ attractors can be equilibria (*stationary regimes*) or limit cycles (*cyclic or periodic regimes*). But in higher-dimensional systems, i.e., for $n \geq 3$, more complex behaviors are possible since attractors can also be *tori (quasi-periodic regimes)* or *strange attractors (chaotic regimes)*.

A torus attracting nearby trajectories is sketched in Figure 3A. A trajectory starting from a point of the torus remains forever on it (i.e., the torus is *invariant* for the dynamics of the system) but, in general, never passes again through the starting point. For example, two frequencies characterize a three-dimensional torus, namely two positive real numbers, $1/T_1$, $1/T_2$, measuring the number of rotations around the cross-section of the torus and the number of revolutions along it, per unit of time. Generically, the ratio T_1/T_2 is irrational, so that there is no period T such that

$$T = T_1 r_1 = T_2 r_2, \quad (2)$$

with r_1 and r_2 positive integers. In words, there is no time T in which a trajectory on the torus carries out an integer number of cross-section rotations and an integer, possibly different, number of torus revolutions, i.e., no time T after which the trajectory revisits the starting point. As a consequence, a single trajectory on the torus covers it densely in the long-run, and the corresponding regime is called quasi-periodic, being the result of two (or more in higher-dimensions) frequencies.

In special cases, however, the ratio T_1/T_2 can be rational, i.e., trajectories on torus can be periodic ($(r_1:r_2)$ *cycles on torus*, for the minimum r_1 and r_2 satisfying (2)). A cycle on torus can be stable (i.e., attracting nearby trajectories on torus) or unstable. For obvious topological reasons, the existence of a stable $(r_1:r_2)$ cycle on torus requires the existence of an unstable $(r_1:r_2)$ cycle on the same torus, and rules out cycles characterized by different pairs.

A strange attractor (a sort of “tangle” in state space) is shown in Figure 3B. Trajectories starting in the vicinity of the tangle tend to it and then remain in it forever. The most striking difference among attractors is that equilibria, cycles, and tori have integer dimension (0, 1, and 2, respectively), while strange attractors are *fractal* sets and therefore have noninteger dimension (see next chapter). Another important difference is that two trajectories starting from very close points in an attractor remain very close forever if the attractor

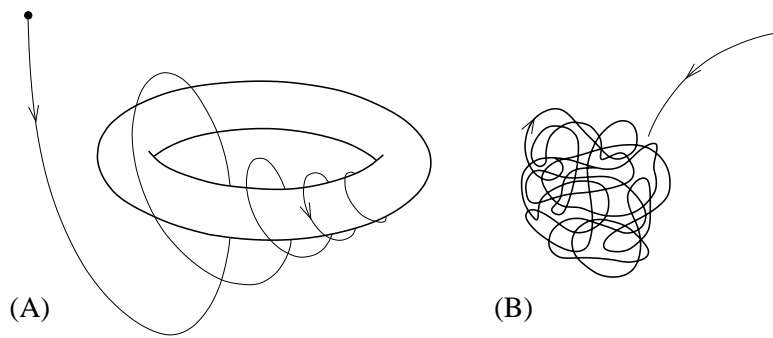


Figure 3: Sketch of an attracting torus (A) and of a strange attractor (B).

is an equilibrium, a cycle, or a torus, while they alternatively diverge (*stretching*) and converge (*folding*) forever if the attractor is a tangle. The mean rate of divergence of nearby trajectories is measured by the so-called *Lyapunov exponents*, and turns out to be the most important indicator in the study of deterministic chaos (see Chapter 14).

In the simple but very important case of linear systems

$$\dot{x}(t) = Ax(t),$$

the state portrait can be immediately obtained from the eigenvalues and eigenvectors of the $n \times n$ matrix A (we recall that the eigenvalues of an $n \times n$ matrix A are the zeros $\lambda_1, \lambda_2, \dots, \lambda_n$ of its characteristic polynomial $\det(\lambda I - A)$, where \det denotes matrix determinant, and that the eigenvectors associated with an eigenvalue λ_i are nontrivial vectors $x^{(i)}$ satisfying the relationship $Ax^{(i)} = \lambda_i x^{(i)}$). There are five generic state portraits of second-order continuous-time linear systems: three of them are shown in Figure 4 (the other two are obtained from cases A and B by reversing the sign of the eigenvalues and all arrows in the state portraits). When the two eigenvalues are complex (case A), the trajectories spiral around the origin and tend to [diverge from] it if the real part of the eigenvalues is negative [positive]. By contrast, when the two eigenvalues are real (cases B and C), the trajectories do not spiral and there are actually special straight trajectories (corresponding to the eigenvectors) converging to [diverging from] the origin if the corresponding eigenvalue is negative [positive]. Along the straight trajectories both state variables vary in time as $\exp(\lambda_i t)$, while along all other trajectories they follow a more complex law of the kind $c_1 \exp(\lambda_1 t) + c_2 \exp(\lambda_2 t)$. Since in generic cases $\lambda_1 \neq \lambda_2$, one of the two exponential functions dominates the other for $t \rightarrow \pm\infty$ and all curved trajectories tend to align with one of the two straight trajectories. In

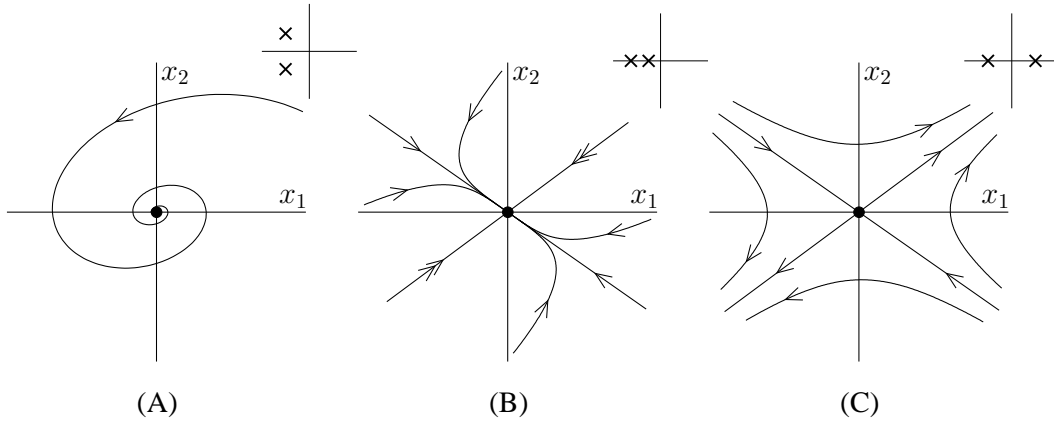


Figure 4: Three state portraits of generic second-order continuous-time linear systems ($\lambda_1 \neq \lambda_2$, both with nonzero real part, see the complex plane associated with each panel): (A) (stable focus) and (B) (stable node) are attractors; the unstable focus (positive real part complex conjugate eigenvalues) and the unstable node (positive real eigenvalues) (repellers) are obtained by reversing all arrows in the state portraits (A) and (B), respectively; (C) is a saddle. Straight trajectories correspond to eigenvectors associated with real eigenvalues. Double arrows indicate the straight trajectories along which the state varies more rapidly.

particular, in the case of a stable node (characterized by $\lambda_2 < \lambda_1 < 0$, see Figure 4B), both exponential functions tend to zero for $t \rightarrow +\infty$, but in the long run $\exp(\lambda_1 t) \gg \exp(\lambda_2 t)$ so that all trajectories, except the two straight trajectories corresponding to the second eigenvector $x^{(2)}$, tend to zero tangentially to the first eigenvector $x^{(1)}$.

Very similar definitions can be given for *discrete-time systems* described by n difference state equations of the form

$$x(t+1) = f(x(t)), \quad (3)$$

where the time t is an integer. In this case trajectories are sequences of points in state space and, again, asymptotic regimes can be stationary, cyclic, quasi-periodic, and chaotic. The major difference between continuous-time and discrete-time dynamical systems is that the former are always *reversible*, since under very general conditions system (1) has a unique solution for $t < 0$, while the latter can be *irreversible*. This implies that discrete-time systems can have quasi-periodic and chaotic regimes even if $n = 1$.

The equilibria of system (1) can be found by determining all solutions \bar{x} of (1) with $\dot{x} = 0$. In second-order systems the equilibria are often determined graphically through the so-called *isoclines*, which are nothing but the lines in state space on which $f_1(x_1, x_2) = 0$ (x_1 -isoclines) and $f_2(x_1, x_2) = 0$ (x_2 -isoclines). Obviously, the equilibria are at the intersections of x_1 - and x_2 -isoclines. Moreover, all trajectories cross x_1 - [x_2 -] isoclines vertically [horizontally] because \dot{x}_1 [\dot{x}_2] is zero on x_1 - [x_2 -] isoclines. This property is often

useful for devising qualitative geometric features of the state portrait.

The stability of an equilibrium \bar{x} is not as easy to ascertain. However, it can very often be discussed through *linearization*, i.e., by approximating the behavior of the system in the vicinity of the equilibrium through a linear system. This can be done in the following way. Let

$$\delta x(t) = x(t) - \bar{x},$$

so that

$$\dot{\delta x}(t) = f(\bar{x} + \delta x(t)).$$

Under very general conditions, we can expand the function f in Taylor series, thus obtaining

$$\dot{\delta x}(t) = f(\bar{x}) + \left. \frac{\partial f}{\partial x} \right|_{x=\bar{x}} \delta x(t) + O(\|\delta x(t)\|^2),$$

where $\|\cdot\|$ is the standard norm in \mathbf{R}^n and $O(\|\delta x(t)\|^2)$ stays for a term that vanishes as $\|\delta x(t)\|^2$ when $\delta x(t) \rightarrow 0$. Noticing that $f(\bar{x}) = 0$, since \bar{x} is a constant solution of (1), we have

$$\dot{\delta x}(t) = \left. \frac{\partial f}{\partial x} \right|_{x=\bar{x}} \delta x(t) + O(\|\delta x(t)\|^2), \quad (4)$$

where the $n \times n$ constant matrix

$$J = \left. \frac{\partial f}{\partial x} \right|_{x=\bar{x}} = \begin{bmatrix} \frac{\partial f_1}{\partial x_1} & \dots & \frac{\partial f_1}{\partial x_n} \\ \vdots & & \vdots \\ \frac{\partial f_n}{\partial x_1} & \dots & \frac{\partial f_n}{\partial x_n} \end{bmatrix}_{x=\bar{x}} \quad (5)$$

is called the *Jacobian matrix* (or, more simply, *Jacobian*). One can easily imagine that, under suitable conditions, the behavior of system (4) (which is still system (1)) can be well approximated in the vicinity of \bar{x} , by the so-called *linearized system*, which, by definition, is

$$\dot{\delta x}(t) = \left. \frac{\partial f}{\partial x} \right|_{x=\bar{x}} \delta x(t). \quad (6)$$

This is, indeed, the case. In particular, it can be shown that if the solution $\delta x(t)$ of (6) tends to 0 for all

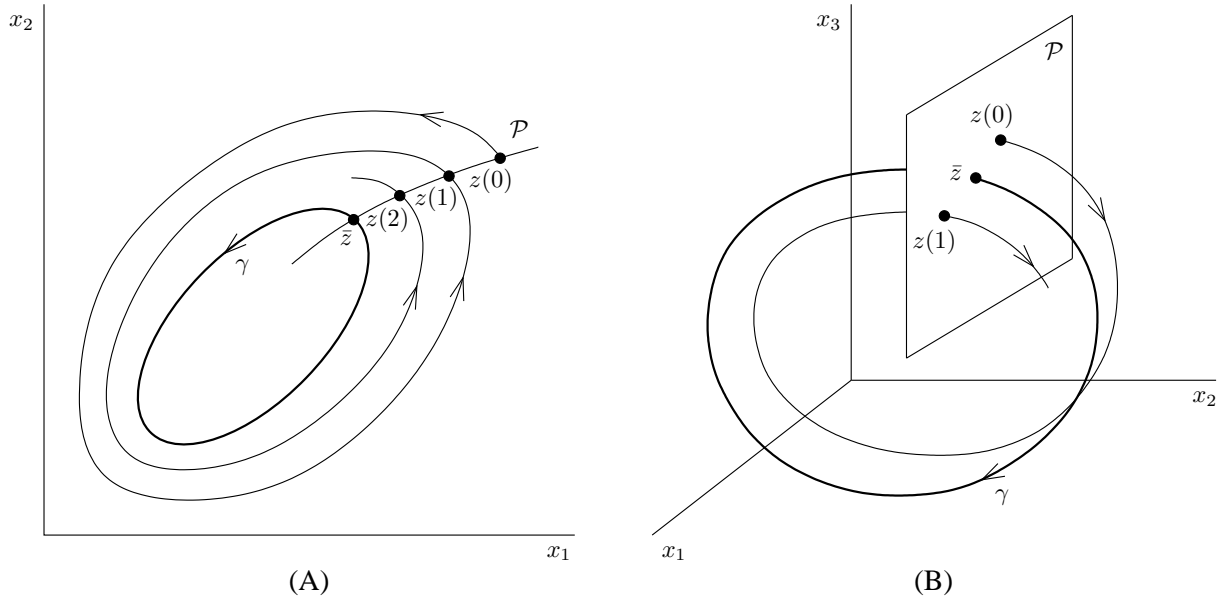


Figure 5: A stable limit cycle γ , the Poincaré section \mathcal{P} , and the sequence $z(0), z(1), z(2), \dots$ of return points.

$\delta x(0) \neq 0$ (as in Figures 4A and B), then the same is true for system (4) provided $\|\delta x(0)\|$ is sufficiently small. In other words, the stability of the linearized system implies the (local) stability of the equilibrium \bar{x} . This result is quite interesting because the stability of the linearized system can be numerically ascertained by checking if all eigenvalues $\lambda_i, i = 1, \dots, n$, of the Jacobian matrix (5) have negative real part. A similar result holds also for the case of unstable equilibria. More precisely, if at least one eigenvalue λ_i of the Jacobian matrix has positive real part (as in Figure 4C), then the equilibrium \bar{x} is locally unstable (i.e., the solution of (4) diverges at least temporarily from zero for suitable $\delta x(0)$, no matter how small $\|\delta x(0)\|$ is). Similarly, the local stability of an equilibrium of a discrete-time system of the form (3) can be studied by simply looking at the module $|\lambda_i|$ of the n eigenvalues λ_i . In fact, if all $|\lambda_i| < 1$, i.e., if all eigenvalues are inside the unit circle in the complex plane, the equilibrium is stable, while if at least one eigenvalue is outside the unit circle ($|\lambda_i| > 1$), the equilibrium is unstable.

The study of the stability of limit cycles can also be carried out through linearization, following a very simple idea suggested by Poincaré (see Figure 5). In the case of second-order systems (see Figure 5A) the Poincaré method consists in cutting locally and transversally the limit cycle with a manifold \mathcal{P} , called the *Poincaré section*, and looking at the sequence $z(0), z(1), z(2), \dots$ of points of return of the trajectory to \mathcal{P} . Since \mathcal{P} is one dimensional, $z(t)$ is a scalar coordinate on \mathcal{P} and the state equation (1) implicitly defines a

first-order discrete-time system called the *Poincaré map*

$$z(t + 1) = P(z(t)). \quad (7)$$

The intersection \bar{z} of the limit cycle γ with \mathcal{P} is an equilibrium of the Poincaré map (since $\bar{z} = P(\bar{z})$) and γ is stable if and only if the equilibrium \bar{z} of (7) is stable. One can therefore use the linearization technique, by taking into account that the eigenvalue of the linearized Poincaré map, $dP/dz|_{z=\bar{z}}$ (called the *Floquet multiplier*, or simply multiplier, of the cycle), cannot be negative, since trajectories cannot cross each other. Thus, a sufficient condition for the (local) stability of the limit cycle γ is

$$\left. \frac{dP}{dz} \right|_{z=\bar{z}} < 1, \quad (8)$$

while the reverse inequality implies the instability of γ .

Similarly, in the case of third-order systems (see Figure 5B) the Poincaré section is a two-dimensional manifold \mathcal{P} and the points of return $z(0), z(1), z(2), \dots$ are generated by a two-dimensional Poincaré map (7). Again, the cycle is stable if and only if the equilibrium \bar{z} of the discrete-time system (7) is stable. Thus, if the two multipliers of the cycle, i.e., the two eigenvalues of the Jacobian matrix $\partial P/\partial z|_{z=\bar{z}}$, are smaller than 1 in module, the cycle γ is stable, while if the module of at least one multiplier is greater than 1 the cycle is unstable. These sufficient conditions for the stability and instability of a cycle can obviously be extended to the n -dimensional case, where $\partial P/\partial z|_{z=\bar{z}}$ is an $(n - 1) \times (n - 1)$ matrix. It must be noticed, however, that they can only be verified numerically, since the cycle γ is, in general, not known analytically.

The Poincaré section is also very useful for distinguishing quasi-periodic from chaotic regimes in third order systems. In fact, a torus appears on a Poincaré section as a regular closed curve, while strange attractors appear as clouds of points (with fractal geometry), as shown in Figure 6.

2 Structural Stability

Structural stability is a key notion in the theory of dynamical systems, since it is needed to understand interesting phenomena like catastrophic transitions, bistability, hysteresis, frequency locking, synchronization, subharmonics, deterministic chaos, as well as many others. The final target of structural stability is the study



Figure 6: The image of a strange attractor on a Poincaré section.

of the asymptotic behavior of parameterized families of dynamical systems of the form

$$\dot{x}(t) = f(x(t), p), \quad (9)$$

for continuous-time systems, and

$$x(t + 1) = f(x(t), p), \quad (10)$$

for discrete-time systems, where p is a vector of constant *parameters*. Given the parameter vector p , all the definitions that we have seen in the previous section apply to the particular dynamical system of the family identified by p . Thus, all geometric and analytical properties of systems (9) and (10), e.g., trajectories, state portrait, equilibria, limit cycles, their stability and associated Jacobian matrices and Poincaré maps, the basins of attraction, and, consequently, the asymptotic behavior of the system, now depend upon p .

Structural stability allows one to rigorously explain why a small change in a parameter value can give rise to a radical change in the system behavior. More precisely, the aim is to find regions \mathcal{P}_i in parameter space characterized by the same qualitative behavior of system (9), in the sense that all state portraits corresponding to values $p \in \mathcal{P}_i$ are topologically equivalent (i.e., they can be obtained one from the other through a simple deformation of the trajectories). Thus, varying $p \in \mathcal{P}_i$ the system conserves all the characteristic elements of the state portrait, namely its attractors, repellers, and saddles. In other words, when p is varied in \mathcal{P}_i , the characteristic frame varies but conserves its structure. Figure 7 shows the typical result of a study of structural stability in the space (p_1, p_2) of two parameters of a second-order system. The parameter space is subdivided into three regions, \mathcal{P}_1 , \mathcal{P}_2 , and \mathcal{P}_3 , and for all interior points of each one of these regions the state portrait is topologically equivalent to that sketched in the figure. In \mathcal{P}_1 the system is an oscillator, since

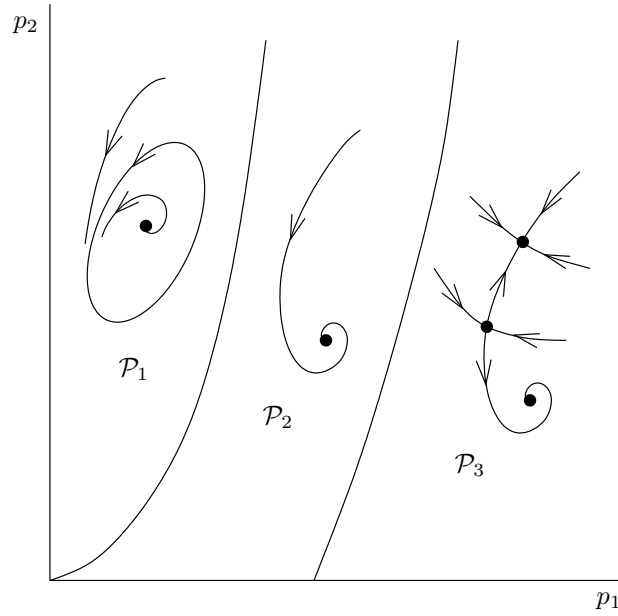


Figure 7: Bifurcation diagram of a second-order system. The curves separating regions \mathcal{P}_1 , \mathcal{P}_2 , and \mathcal{P}_3 are bifurcation curves.

it has a single attractor, which is a limit cycle. Also in \mathcal{P}_2 there is a single attractor, which is, however, an equilibrium. Finally, in \mathcal{P}_3 we have *bistability* since the system has two alternative attractors (two equilibria), each with its own basin of attraction delimited by the stable manifold of the saddle equilibrium.

If p is an interior point of a region \mathcal{P}_i , system (9) is said to be *structurally stable* at p since its state portrait is qualitatively the same as those of the systems obtained by slightly perturbing the parameters in all possible ways. By contrast, if p is on the boundary of a region \mathcal{P}_i the system is not structurally stable since small perturbations can give rise to qualitatively different state portraits. The points of the boundaries of the regions \mathcal{P}_i are called *bifurcation points*, and, in the case of two parameters, the boundaries are called *bifurcation curves*. Bifurcation points are therefore points of degeneracy. If they lie on a curve separating two distinct regions \mathcal{P}_i and \mathcal{P}_j , $i \neq j$, they are called codimension-1 bifurcation points, while if they lie on the boundaries of three distinct regions they are called codimension-2 bifurcation points, and so on.

Notice that the simplest dynamical system, namely the first-order linear system $\dot{x}(t) = px(t)$, has a bifurcation at $p = p^* = 0$, i.e., when its eigenvalue p is equal to zero. In fact, such a system is stable for $p < 0$ and unstable for $p > 0$, while it is neutrally stable (i.e., the equilibrium $x = 0$ is not unstable but does not attract all nearby trajectories) for $p = p^* = 0$.

In the following, we mainly focus on second-order, continuous-time systems and limit the discussion to

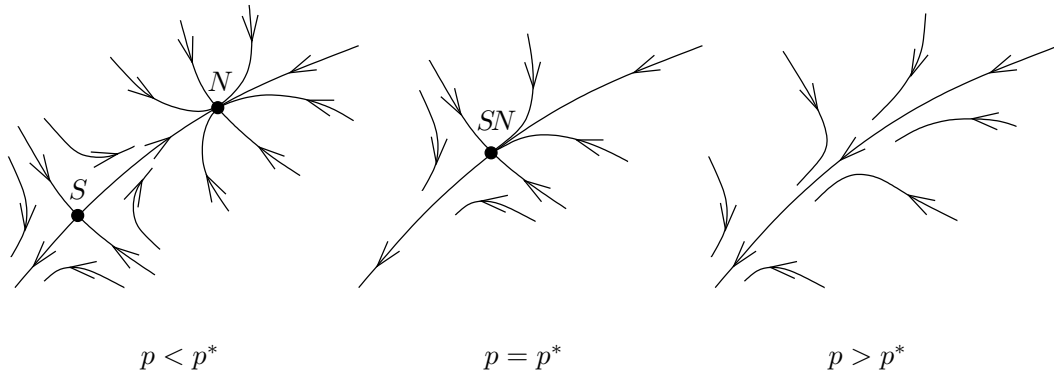


Figure 8: Example of local bifurcation: saddle-node bifurcation.

codimension-1 bifurcations.

3 Bifurcations as Collisions

A generic element of the parameterized family of dynamical systems (9) must be imagined to be structurally stable because if p is selected randomly it will be an interior point of a region \mathcal{P}_i with probability 1. In generic conditions, attractors, repellers, saddles, and their stable and unstable manifolds are separated one from each other. Moreover, the eigenvalues of the Jacobian matrices associated with equilibria have nonzero real parts, while the eigenvalues of linearized Poincaré maps associated with cycles have module different from 1. By continuity, small parametric variations will induce small variations of all attractors, repellers, saddles, and their stable and unstable manifolds which, however, will remain separated if the parametric variations are sufficiently small. The same holds for the eigenvalues of Jacobian matrices and linearized Poincaré maps, which, for sufficiently small parametric variations, will continue to be noncritical. Thus, in conclusion, starting from a generic condition, it is necessary to vary the parameters of a finite amount to obtain a bifurcation, which is generated by the collision of two or more elements of the characteristic frame, which then changes its structure at the bifurcation, thus involving a change of the state portrait of the system.

A bifurcation is called *local* when it involves the degeneracy of some eigenvalue of the Jacobians associated with equilibria or cycles. For example, the bifurcation described in Figure 8, called *saddle-node bifurcation*, is a local bifurcation. Indeed, the bifurcation can be viewed as the collision, at $p = p^*$, of two equilibria: for $p < p^*$ the two equilibria (elements of the characteristic frame) are distinct and one is stable (the node N) while the other is unstable (the saddle S). Then, as p increases, the two equilibria approach

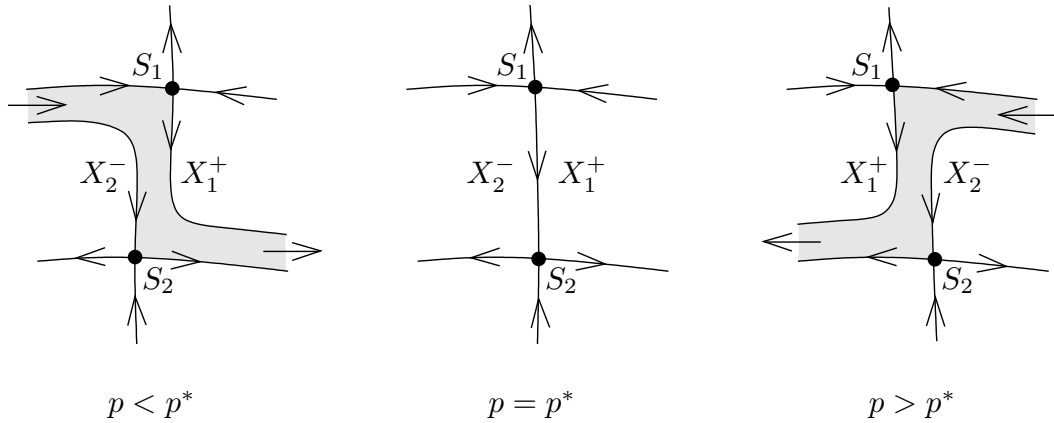


Figure 9: Example of global bifurcation: heteroclinic bifurcation.

one each other and finally collide when $p = p^*$ (and then disappear). Notice that the characteristic frame is degenerate at $p = p^*$ because it is composed of one element (an equilibrium), while there are two equilibria for $p < p^*$ and none for $p > p^*$. But the bifurcation can also be interpreted in terms of eigenvalue degeneracy. In fact, the eigenvalues of the Jacobian evaluated at the saddle are one positive and one negative, while the eigenvalues of the Jacobian evaluated at the node are both negative, so that when the two equilibria coincide, one of the two eigenvalues of the unique Jacobian matrix must be equal to zero.

By contrast, *global bifurcations* cannot be revealed by eigenvalue degeneracies. One example, known as *heteroclinic bifurcation*, is shown in Figure 9, which presents the characteristic frames (two saddles and their stable and unstable manifolds) of a system for $p = p^*$ (bifurcation value) and for $p \neq p^*$. The characteristic frame for $p = p^*$ is structurally different from the others because it corresponds to the collision of the unstable manifold X_1^+ of the first saddle with the stable manifold X_2^- of the second saddle. However, the two Jacobian matrices associated with the two saddles do not degenerate at p^* , since their eigenvalues remain different from zero. In other words, the bifurcation cannot be revealed by the behavior of the system in the vicinity of an equilibrium, but is the result of the global behavior of the system.

When there is only one parameter p and there are various bifurcations at different values of the parameter, it is often advantageous to represent the dependence of the system behavior upon the parameter by drawing in the three-dimensional space (p, x_1, x_2) , often called *control space*, the characteristic frame for all values of p . This is done, for example, in Figure 10 for the same system described in Figure 7, with $p = p_1$ and constant p_2 . Figure 10 shows that for increasing values of p a so-called *Hopf bifurcation* occurs, as the stable limit cycle shrinks to a point, thus colliding with the unstable equilibrium that exists inside the cycle. This

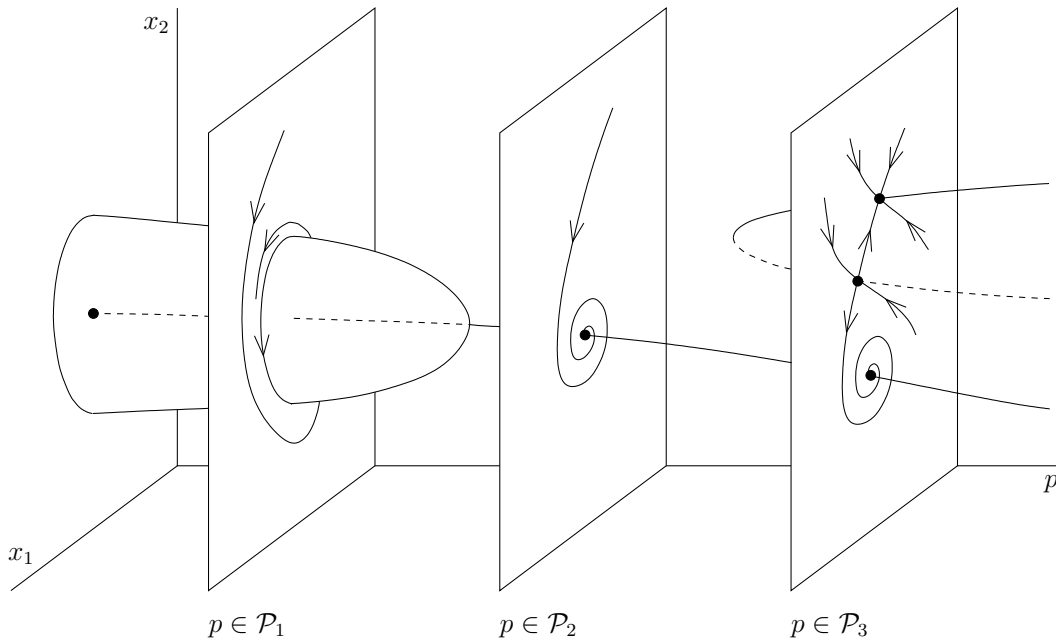


Figure 10: Characteristic frame in the control space of a system with a Hopf and a saddle-node bifurcation. Continuous lines represent trajectories in the three illustrated state portraits and stable equilibria or limit cycles otherwise; dashed lines represent unstable equilibria. The symbols \mathcal{P}_1 , \mathcal{P}_2 , and \mathcal{P}_3 refer to Figure 7.

is a local bifurcation, because the equilibrium is stable for higher values of p , so that the bifurcation can be revealed by an eigenvalue degeneracy. The figure also shows that a saddle-node bifurcation occurs at a higher value of the parameter, as two equilibria, namely a stable node and a saddle, become closer and closer until they collide and disappear. The Hopf and the saddle-node bifurcations are perhaps the most popular local bifurcations of second-order systems and are discussed in some detail in the next section.

4 Local Bifurcations

In this section we discuss the seven most important local bifurcations of continuous-time systems. Three of them, called *transcritical*, saddle-node (already encountered above), and *pitchfork*, can be viewed as collisions of equilibria. Since they can occur in first-order systems, we present them in that context. The other bifurcations involve limit cycles. Two of them can occur in second-order systems, namely the Hopf bifurcation (already seen), i.e., the collision of an equilibrium with a vanishing cycle, and the *tangent of limit cycles*, which is the collision of two cycles. The last two bifurcations, the *flip* (or *period-doubling*) and the *Neimark-Sacker* (or *torus*), are more complex because they can occur only in three- (or higher-) dimensional systems. The first is a particular collision of two limit cycles, one with period double than the other, while

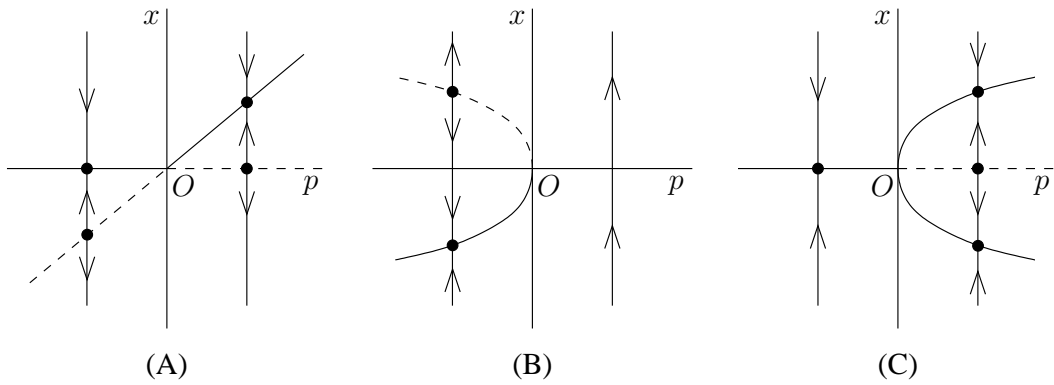


Figure 11: Three local bifurcations viewed as collisions of equilibria: (A) transcritical; (B) saddle-node; (C) pitchfork.

the second is the collision between a cycle and a vanishing torus.

Transcritical, Saddle-Node, and Pitchfork Bifurcations

Figure 11 shows three different types of collisions of equilibria in first-order systems of the form (9). The state x and the parameter p have been normalized in such a way that the bifurcation occurs at $p^* = 0$ and that the corresponding equilibrium is zero. Continuous lines in the figure represent stable equilibria, while dashed lines indicate unstable equilibria. In Figure 11A the collision is visible in both directions, while in Figures 11B and C the collision is visible only from the left or from the right. The three bifurcations are called, respectively, transcritical, saddle-node, and pitchfork, and the three most simple state equations (called *normal forms*) giving rise to Figure 11 are

$$\dot{x}(t) = px(t) - x^2(t), \quad \text{transcritical}, \quad (11a)$$

$$\dot{x}(t) = p + x^2(t), \quad \text{saddle-node}, \quad (11b)$$

$$\dot{x}(t) = px(t) - x^3(t), \quad \text{pitchfork}. \quad (11c)$$

The first of these bifurcations is also called *exchange of stability* since the two equilibria exchange their stability at the bifurcation. The second is called saddle-node bifurcation because in second-order systems it corresponds to the collision of a saddle with a node, as shown in Figure 8, but it is also known as *fold*, in view of the form of the graph of its equilibria. Due to the symmetry of the normal form, the pitchfork has three colliding equilibria, two stable and one unstable in the middle.

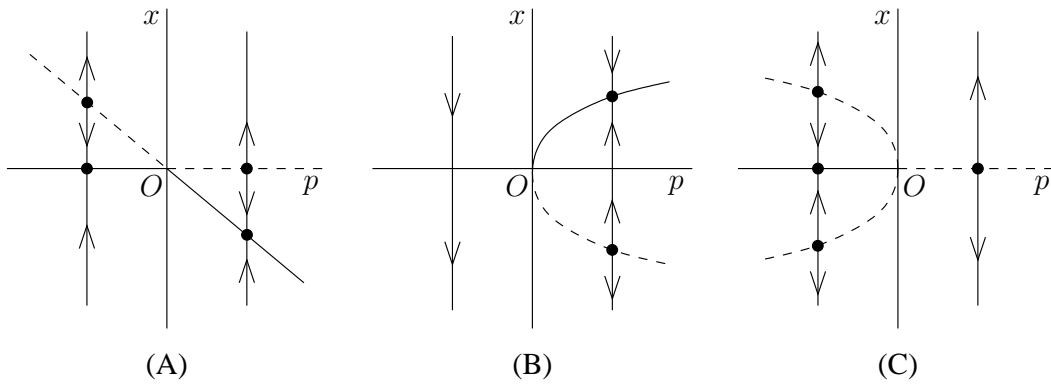


Figure 12: Bifurcation diagrams corresponding to the normal forms (12).

It is worth noticing that in changing the sign of the quadratic and cubic terms in the normal forms (11), three new normal forms are obtained, namely

$$\dot{x}(t) = px(t) + x^2(t), \quad \text{transcritical}, \quad (12a)$$

$$\dot{x}(t) = p - x^2(t), \quad \text{saddle-node}, \quad (12b)$$

$$\dot{x}(t) = px(t) + x^3(t), \quad \text{pitchfork}, \quad (12c)$$

which have the bifurcation diagrams shown in Figure 12. Comparing Figures 11 and 12, it is easy to verify that nothing changes from a phenomenological point of view in the first two cases. However, for the pitchfork bifurcation this is not true, since in case (11c) there is at least one attractor for each value of the parameter, while in case (12c), for $p > 0$, there is only a repellor. To distinguish the two possibilities, the pitchfork (11c) is called *supercritical*, while the other is called *subcritical*.

Hopf Bifurcation

The Hopf bifurcation (actually discovered by A. A. Andronov for second-order systems; see Andronov *et al.*, 1973, and Marsden & McCracken, 1976, for the English translation of Andronov and Hopf's original works) explains how a stationary regime can become cyclic as a consequence of a small variation of a parameter, a rather common phenomenon not only in physics but also in biology, economics, and life sciences. In terms of collisions, this bifurcation involves an equilibrium and a cycle which, however, shrinks to a point when the collision occurs. Figure 13 shows the two possible cases, known as supercritical and subcritical Hopf bifurcations, respectively. In the supercritical case, a stable cycle has in its interior an unstable focus. When

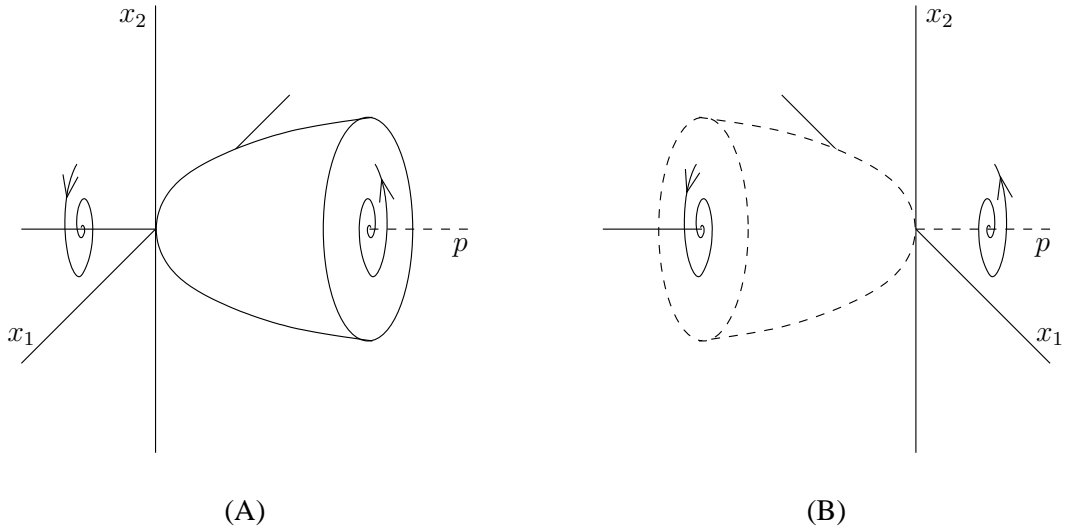


Figure 13: Hopf bifurcation: (A) supercritical; (B) subcritical.

the parameter is varied the cycle shrinks until it collides with the equilibrium and after the collision only a stable equilibrium remains. By contrast, in the subcritical case the cycle is unstable and is the boundary of the basin of attraction of the stable equilibrium inside the cycle. Thus, after the collision there is only a repeller.

The normal form of the Hopf bifurcation is

$$\begin{aligned}\dot{x}_1(t) &= px_1(t) - \omega x_2(t) + cx_1(t)(x_1^2(t) + x_2^2(t)), \\ \dot{x}_2(t) &= \omega x_1(t) + px_2(t) + cx_2(t)(x_1^2(t) + x_2^2(t)),\end{aligned}$$

which, in polar coordinates, becomes

$$\begin{aligned}\dot{\rho}(t) &= p\rho(t) + c\rho^3(t), \\ \dot{\theta}(t) &= \omega.\end{aligned}$$

This last form shows that the trajectory spirals around the origin at constant angular velocity ω , while the distance from the origin varies in accordance with the first ODE, which is the normal form of the pitchfork. Thus, the stability of the cycle depends upon the sign of c , called the *Lyapunov coefficient*.

Taking into account Figures 11C and 12C, it is easy to check that the Hopf bifurcation is supercritical [subcritical] if $c < 0$ [$c > 0$] (in the case $c = 0$ the system is linear and for $p = p^* = 0$ the origin is

neutrally stable and surrounded by an infinity of cycles). For $p = p^*$ the origin of the state space is stable in the supercritical case and unstable in the opposite case. The Jacobian of the normal form, evaluated at the origin, is

$$J = \begin{bmatrix} p & -\omega \\ \omega & p \end{bmatrix},$$

and its two eigenvalues $\lambda_{1,2} = p \pm i\omega$ cross the imaginary axis of the complex plane when $p = 0$. This is the property commonly used to detect Hopf bifurcations in second-order systems. In fact, denoting by $\bar{x}(p)$ an equilibrium of the system, the Jacobian evaluated at $\bar{x}(p)$ is

$$J = \begin{bmatrix} \frac{\partial f_1}{\partial x_1} & \frac{\partial f_1}{\partial x_2} \\ \frac{\partial f_2}{\partial x_1} & \frac{\partial f_2}{\partial x_2} \end{bmatrix}_{x=\bar{x}(p)},$$

and such a matrix has a pair of nontrivial and purely imaginary eigenvalues if and only if

$$\begin{aligned} \text{trace}(J) &= \frac{\partial f_1}{\partial x_1} \Big|_{x=\bar{x}(p)} + \frac{\partial f_2}{\partial x_2} \Big|_{x=\bar{x}(p)} = 0, \\ \det(J) &= \frac{\partial f_1}{\partial x_1} \Big|_{x=\bar{x}(p)} \frac{\partial f_2}{\partial x_2} \Big|_{x=\bar{x}(p)} - \frac{\partial f_1}{\partial x_2} \Big|_{x=\bar{x}(p)} \frac{\partial f_2}{\partial x_1} \Big|_{x=\bar{x}(p)} > 0. \end{aligned}$$

In practice, one annihilates the trace of the Jacobian evaluated at the equilibrium and finds in this way the parameter values that are candidate Hopf bifurcations. Then, the test on the positivity of the determinant of J is used to select the true Hopf bifurcations among the candidates. Under suitable nondegeneracy conditions, the emerging cycle is unique and its frequency is $\omega = \sqrt{\det(J)}$, because $\sqrt{\det(J)} = \lambda_1 \lambda_2$, while its amplitude increases as $\sqrt{-c(p - p^*)}$.

Determining if a Hopf bifurcation is supercritical or subcritical is not easy. One can try to find out if the equilibrium is stable or unstable but this is quite difficult since linearization is unreliable at a bifurcation. Alternatively (but equivalently), one can determine the sign of the Lyapunov coefficient c by following a procedure that is often quite cumbersome [see, e.g., Guckenheimer & Holmes, 1997, Kuznetsov, 2004] and is therefore not reported here.

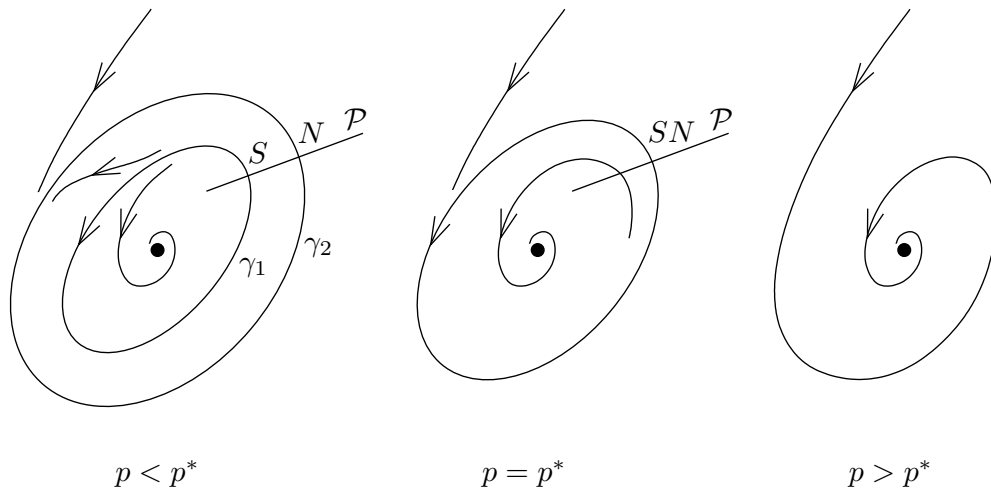


Figure 14: Tangent bifurcation of limit cycles: two cycles γ_1 and γ_2 collide for $p = p^*$ and then disappear.

Tangent Bifurcation of Limit Cycles

Other local bifurcations in second-order systems involve limit cycles and are somehow similar to transcritical, saddle-node, and pitchfork bifurcations of equilibria. In fact, the collision of two limit cycles can be studied as the collision of the two corresponding equilibria of the Poincaré map defined on a Poincaré section cutting both cycles. Thus, the transcritical, saddle-node, and pitchfork bifurcations of such equilibria correspond to analogous bifurcations of the colliding limit cycles.

The most common case is the saddle-node bifurcation of limit cycles, more often called fold or tangent bifurcation of limit cycles, where two cycles collide for $p = p^*$ and then disappear, as shown in Figure 14. On the Poincaré section \mathcal{P} the bifurcation is revealed by the collision of two equilibria of the Poincaré map, S unstable and N stable, which then disappear. In terms of eigenvalue degeneracy, the eigenvalue of the linearized Poincaré map evaluated at S [N] is larger [smaller] than 1, so that when the two equilibria coincide, the eigenvalue of the unique linearized Poincaré map must be equal to 1.

Varying the parameter in the opposite direction, this bifurcation explains the sudden birth of a pair of cycles, one of which is stable. While in the case of the Hopf bifurcation the emerging cycle is degenerate (it has zero amplitude), in this case the emerging cycles are not degenerate.

Flip (Period-doubling) Bifurcation

The flip bifurcation is the collision of two particular limit cycles, one tracing twice the other and therefore having double period, in a three- (or higher-) dimensional state space. In the supercritical [subcritical] case,

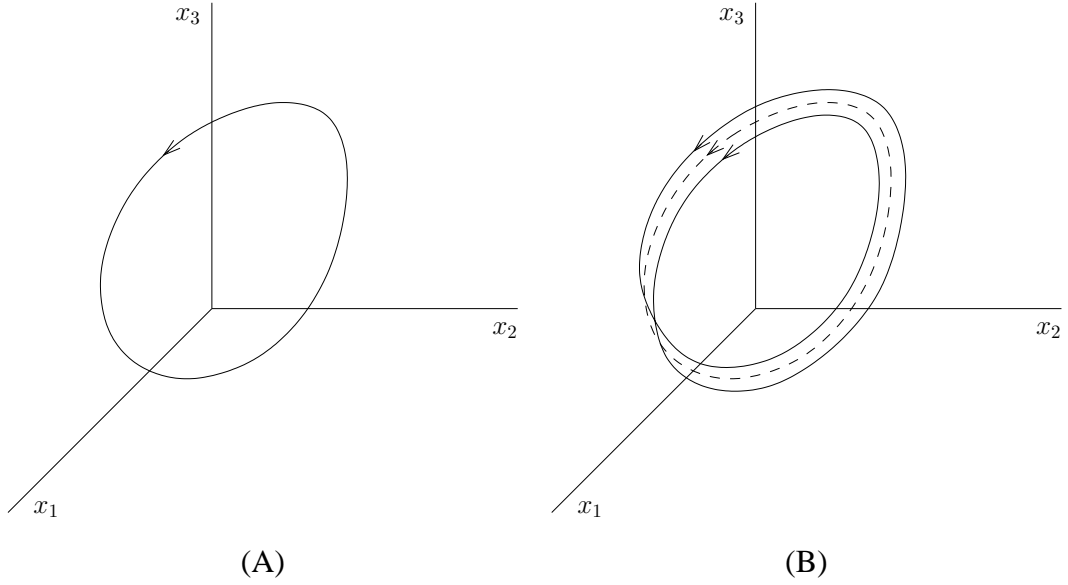


Figure 15: Flip bifurcation: (A) stable limit cycle of period T ; (B) unstable limit cycle of period T and stable limit cycle of period $2T$.

it corresponds to a bifurcation of a stable [unstable] limit cycle of period T into a stable [unstable] limit cycle of period $2T$ and an unstable [stable] limit cycle of period T , as sketched in Figure 15 (for the supercritical case) just before and after the bifurcation.

Physically speaking, the stable limit cycle becomes only slightly different, but the key feature is that the period of the limit cycle doubles through the bifurcation. In other words, if before the bifurcation the graph of one of the state variables, say x_1 , has a single peak in each period T , after the bifurcation the graph has two slightly different peaks in each period $2T$. On a Poincaré section, looking only at second return points, the flip bifurcation resembles the pitchfork bifurcation, where two stable equilibria, \bar{z}' and \bar{z}'' (corresponding to the two intersections of the period- $2T$ cycle with the Poincaré section), collides with a third unstable equilibrium \bar{z} (the intersection of the period- T cycle) and disappear, while \bar{z} becomes stable.

Mathematically speaking, the flip bifurcation is characterized by a multiplier of the period- T cycle equal to -1 . In fact, when the cycle is unstable, the divergence from it, seen on a Poincaré section, is characterized by (first) return points which tend to alternate between points \bar{z}' and \bar{z}'' . This is due to a negative multiplier < -1 . Just after the bifurcation (from right to left in Figure 15), the cycle is stable but the multiplier is still negative, between -1 and 0 , i.e., the multiplier is equal to -1 at the bifurcation.

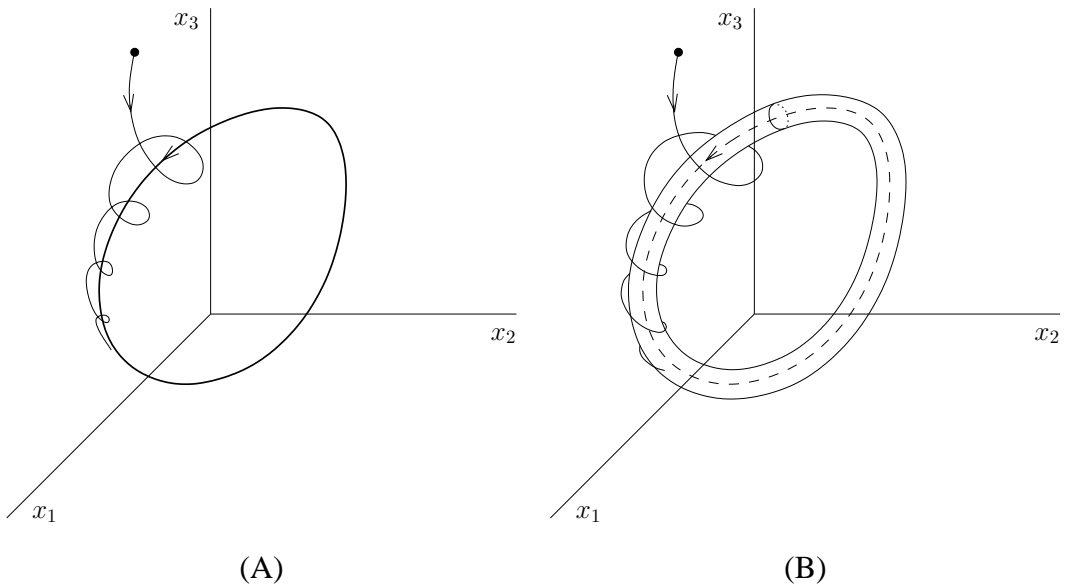


Figure 16: Neimark-Sacker bifurcation: (A) stable limit cycle; (B) unstable limit cycle and small stable torus.

Neimark-Sacker (Torus) Bifurcation

This bifurcation, when supercritical, explains how a stable limit cycle can become a stable torus, by slightly varying a parameter. Figure 16 clearly represents this bifurcation and shows that it can be interpreted (from right to left) as the collision of a stable vanishing torus with an unstable limit cycle inside the torus. On a Poincaré section, one would see a stable equilibrium (intersection of the cycle of Figure 16A with the Poincaré section) bifurcating into an unstable equilibrium and a small regular closed curve (the intersection of the torus of Figure 16B with the Poincaré section). In a sense, on the Poincaré section, one would observe invariant sets with the same geometry observed in the case of the supercritical Hopf bifurcation (see Figure 13A). For this reason, the Neimark-Sacker bifurcation is sometimes confused with the Hopf bifurcation. Similarly, the subcritical Neimark-Sacker bifurcation resembles the subcritical Hopf bifurcation (see Figure 13B).

In terms of cycle multipliers, the Neimark-Sacker bifurcation corresponds to a pair of complex conjugate multipliers crossing the unit circle in the complex plane. When the cycle is stable, nearby trajectories converge to the cycle by spiraling around it, while, when unstable, trajectories diverge from the cycle and spiral toward the torus.

In a two-parameter space, the Neimark-Sacker bifurcation curve separates the region in which the system has periodic regimes from that in which the asymptotic regime is quasi-periodic. However, as shown in

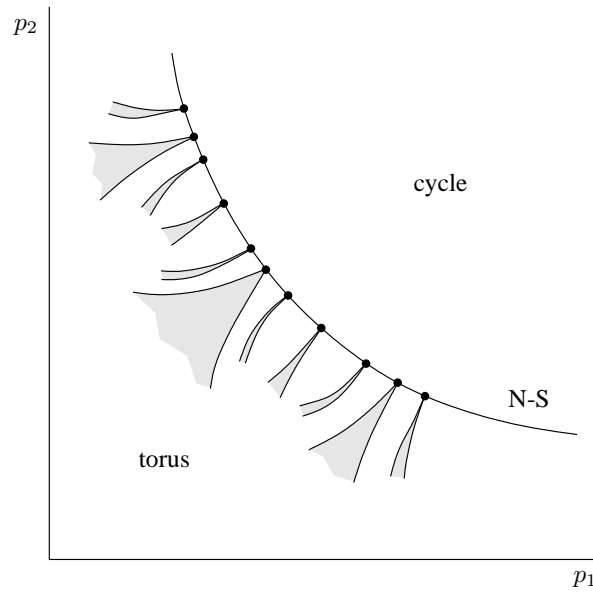


Figure 17: Neimark-Sacker bifurcation curve and Arnold's tongues emanating from it.

Figure 17, in the region where the attractor is a torus, there are very narrow subregions, each delimited by two curves merging on the Neimark-Sacker curve. In these subregions, called *Arnold's tongues*, the attractor is a cycle on torus, and the two curves delimiting each tongue are tangent bifurcations of limit cycles. The points on the Neimark-Sacker curve from which the Arnold's tongues emanate are therefore codimension-2 bifurcation points. Although the Arnold's tongues are infinitely many, but countable (generically, there is a tongue for each possible $(r_1 : r_2)$ pair characterizing a cycle on torus), only a few of them can be numerically or experimentally detected, since the others are too thin. Nevertheless, the Arnold's tongues are quite important because they explain the subtle and intriguing phenomenon known as *frequency locking*.

5 Global Bifurcations

As already said in Section 3, global bifurcations cannot be detected through the analysis of the Jacobians associated with equilibria or cycles. However, they can still be viewed as structural changes of the characteristic frame.

Heteroclinic Bifurcation

In Figure 9 we have already reported the bifurcation corresponding to the collision of a stable manifold of a saddle with the unstable manifold of another saddle. This bifurcation is called heteroclinic bifurcation,

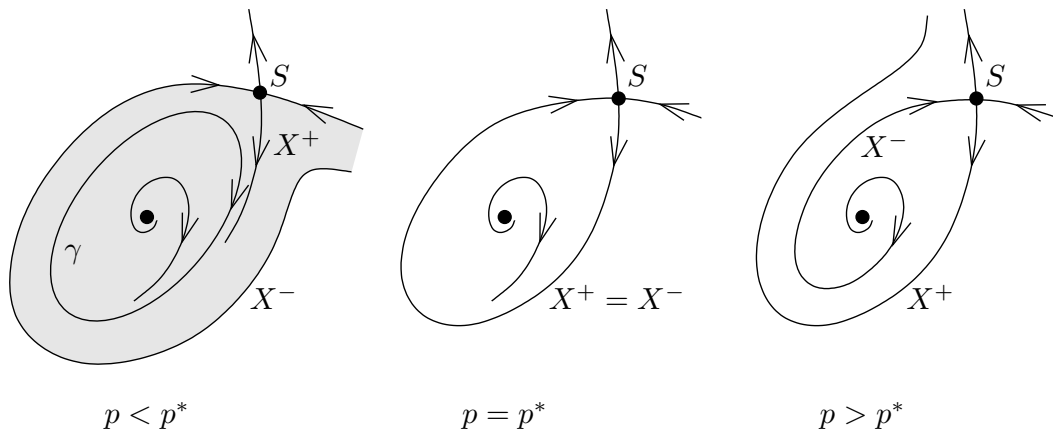


Figure 18: Homoclinic bifurcation to standard saddle: for $p = p^*$ the stable manifold X^- of the saddle S collides with the unstable manifold X^+ of the same saddle. The bifurcation can also be viewed as the collision of the cycle γ with the saddle S .

since the trajectory connecting the two saddles is called heteroclinic trajectory (or connection).

Homoclinic Bifurcation

A special but important global bifurcation is the so-called *homoclinic bifurcation*, characterized by the presence of a trajectory connecting an equilibrium with itself, called homoclinic trajectory (or connection).

There are two collisions that give rise to a homoclinic trajectory. The first and most common collision is that between the stable and unstable manifolds of the same saddle, as depicted in Figure 18. The second collision, shown in Figure 19, is that between a node and a saddle whose unstable manifold is connected to the node. The corresponding bifurcations are called *homoclinic bifurcation to standard saddle*, or simply homoclinic bifurcation, and *homoclinic bifurcation to saddle-node*.

Figure 18 shows that the homoclinic bifurcation to standard saddle can also be viewed as the collision of a cycle $\gamma(p)$ with a saddle $S(p)$. When p approaches p^* the cycle $\gamma(p)$ gets closer and closer to the saddle $S(p)$, so that the period $T(p)$ of the cycle becomes longer and longer, since the state of the system moves very slowly when it is very close to the saddle. By contrast, Figure 19 shows that the homoclinic bifurcation to saddle-node can be viewed as a saddle-node bifurcation on a cycle $\gamma(p)$, which therefore disappears. When p approaches p^* the system “feels” the forthcoming appearance of the two equilibria and therefore the state slows down close to the point where they are going to appear. Thus, in both cases, $T(p) \rightarrow \infty$ as $p \rightarrow p^*$ and this property is often used to detect homoclinic bifurcations through simulation. Another property used to detect homoclinic bifurcations to standard saddles through simulation is related to the form

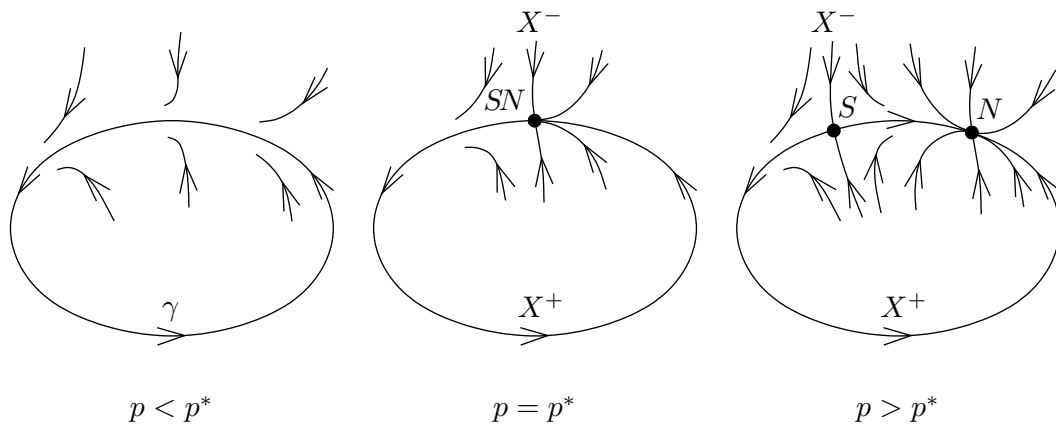


Figure 19: Homoclinic bifurcation to saddle-node: for $p = p^*$ the unstable manifold X^+ of the saddle-node SN comes back to SN transversally to the stable manifold X^- . The bifurcation can also be viewed as a saddle-node bifurcation on the cycle γ .

of the limit cycle which becomes “pinched” close to the bifurcation, the angle of the pinch being the angle between the stable and unstable manifolds of the saddle.

Looking at Figures 18 and 19 from the right to the left, we can recognize that the homoclinic bifurcation explains the birth of a limit cycle. As in the case of Hopf bifurcations, the emerging limit cycle is degenerate, but this time the degeneracy is not in the amplitude of the cycle but in its period, which is infinitely long. The emerging limit cycles are stable in the figures (the gray region in Figure 18 is the basin of attraction), but reversing the arrows of all trajectories the same figures could be used to illustrate the cases of unstable emerging cycles. In other words, homoclinic bifurcations in second-order systems are generically associated with a cycle emerging from the homoclinic trajectory existing at $p = p^*$ by suitably perturbing the parameter. It is interesting to note that the stability of the emerging cycle can be easily predicted by looking at the sign of the so-called *saddle quantity* σ , which is the sum of the two eigenvalues of the Jacobian matrix associated with the saddle, i.e., the trace of the Jacobian (notice that one eigenvalue is equal to zero in the case of homoclinic bifurcation to saddle-node). More precisely, if $\sigma < 0$ the cycle is stable, while if $\sigma > 0$ the cycle is unstable. As proved by Andronov and Leontovich [see Andronov *et al.*, 1973], this result holds under a series of assumptions that essentially rule out a number of critical cases. A very important and absolutely not simple extension of Andronov and Leontovich theory is Shil’nikov theorem [Shil’nikov, 1968] concerning homoclinic bifurcations in three-dimensional systems.

6 Catastrophes, Hysteresis, and Cusp

We can now present a simple but comprehensive treatment of a delicate problem, that of *catastrophic transitions* in dynamical systems. A lot has been said on this topic in the last decades and the so-called *catastrophe theory* [Thom, 1972] has often been invoked improperly, thus generating expectations that will never be satisfied. Reduced to its minimal terms, the problem of catastrophic transitions is the following: assuming that a system is functioning in one of its asymptotic regimes, is it possible that a microscopic variation of a parameter triggers a transient toward a macroscopically different asymptotic regime? When this happens, we say that a catastrophic transition occurs.

To be more specific, assume that an instantaneous small perturbation from p to $p + \Delta p$ occurs at time $t = 0$ when the system is on one of its attractors, say $\mathcal{A}(p)$, or at a point $x(0)$ very close to $\mathcal{A}(p)$ in the basin of attraction $B(\mathcal{A}(p))$. A first possibility is that p and $p + \Delta p$ are not separated by any bifurcation. This implies that the state portrait of the perturbed system $\dot{x} = f(x, p + \Delta p)$ can be obtained by slightly deforming the state portrait of the original system $\dot{x} = f(x, p)$. In particular, if Δp is small, by continuity, the attractors $\mathcal{A}(p)$ and $\mathcal{A}(p + \Delta p)$, as well as their basins of attraction $B(\mathcal{A}(p))$ and $B(\mathcal{A}(p + \Delta p))$, are almost coincident, so that $x(0) \in B(\mathcal{A}(p + \Delta p))$. This means that after the perturbation a transition will occur from $\mathcal{A}(p)$ (or $x(0)$ close to $\mathcal{A}(p)$) to $\mathcal{A}(p + \Delta p)$. In conclusion, a microscopic variation of a parameter has generated a microscopic variation in system behavior.

The opposite possibility is that p and $p + \Delta p$ are separated by a bifurcation. In such a case it can happen that the small parameter variation triggers a transient, bringing the system toward a macroscopically different attractor. When this happens for all initial states $x(0)$ close to $\mathcal{A}(p)$, the bifurcation is called *catastrophic*. By contrast, if the catastrophic transition is not possible, the bifurcation is called *noncatastrophic*, while in all other cases the bifurcation is said to be *undetermined*.

We can now revisit all bifurcations we have discussed in the previous sections. Let us start with Figure 11 and assume that p is small and negative, i.e., $p = -\epsilon$, that $x(0)$ is different from zero but very small, i.e., close to the stable equilibrium, and that $\Delta p = 2\epsilon$ so that, after the perturbation, $p = \epsilon$. In case A (transcritical bifurcation) $x(t) \rightarrow \epsilon$ if $x(0) > 0$ and $x(t) \rightarrow -\infty$ if $x(0) < 0$. Thus, this bifurcation is undetermined because it can, but does not always, give rise to a catastrophic transition. In a case like this, the noise acting on the system has a fundamental role since it determines the sign of $x(0)$, which is crucial for the behavior of the system after the parametric perturbation. We must notice, however, that in many cases the sign of $x(0)$

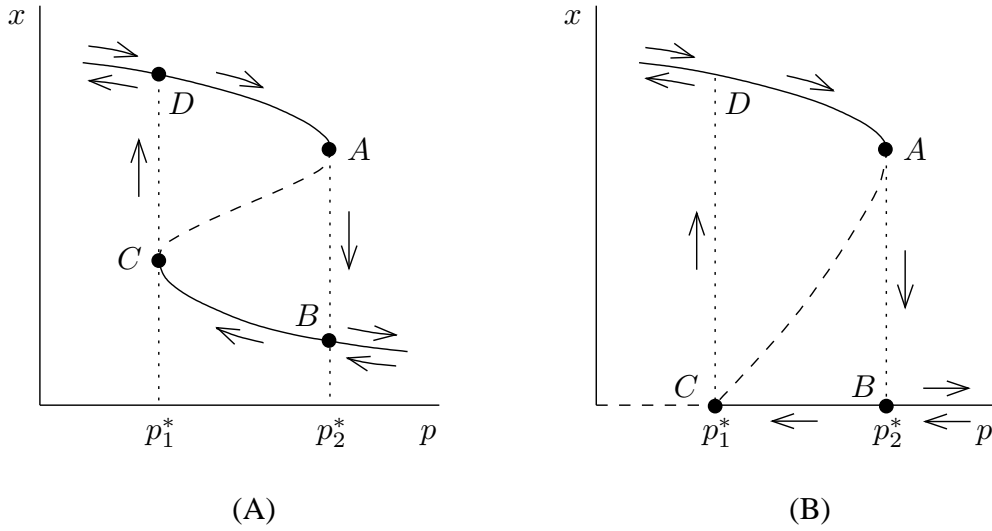


Figure 20: Two systems with hysteresis generated by two saddle-node bifurcations (A), and a saddle-node and a transcritical bifurcation (B).

is a priori fixed. For example, if the system is positive because x represents the density of a population, then for physical reasons $x(0) > 0$ and the bifurcation is therefore noncatastrophic. However, under the same conditions, the transcritical bifurcation of Figure 12A is catastrophic. Similarly, we can conclude that the saddle-node bifurcation of Figure 11B is catastrophic, as well as that of Figure 12B, and that the pitchfork bifurcation can be noncatastrophic (as in Figure 11C) or catastrophic (as in Figure 12C).

From Figure 13 we can immediately conclude that the supercritical Hopf bifurcation is noncatastrophic, while the subcritical one is catastrophic. This is why the two Hopf bifurcations are sometimes called catastrophic and noncatastrophic. Finally, Figures 14, 18, and 19 show that tangent and homoclinic bifurcations are catastrophic.

When a small parametric variation triggers a catastrophic transition from an attractor \mathcal{A}' to an attractor \mathcal{A}'' it is interesting to determine if it is possible to drive the system back to the attractor \mathcal{A}' by suitably varying the parameter. When this is possible, the catastrophe is called *reversible*. The most simple case of reversible catastrophes is the *hysteresis*, two examples of which (concerning first-order systems) are shown in Figure 20. In case A the system has two saddle-node bifurcations, while in case B there is a transcritical bifurcation at p_1^* and a saddle-node bifurcation at p_2^* . All bifurcations are catastrophic (because the transitions $A \rightarrow B$ and $C \rightarrow D$ are macroscopic) and if p is varied back and forth between $p_{\min} < p_1^*$ and $p_{\max} > p_2^*$ through a sequence of small steps with long time intervals between successive steps, the state of the system follows closely the cycle $A \rightarrow B \rightarrow C \rightarrow D$ indicated in the figure and called *hysteretic*.

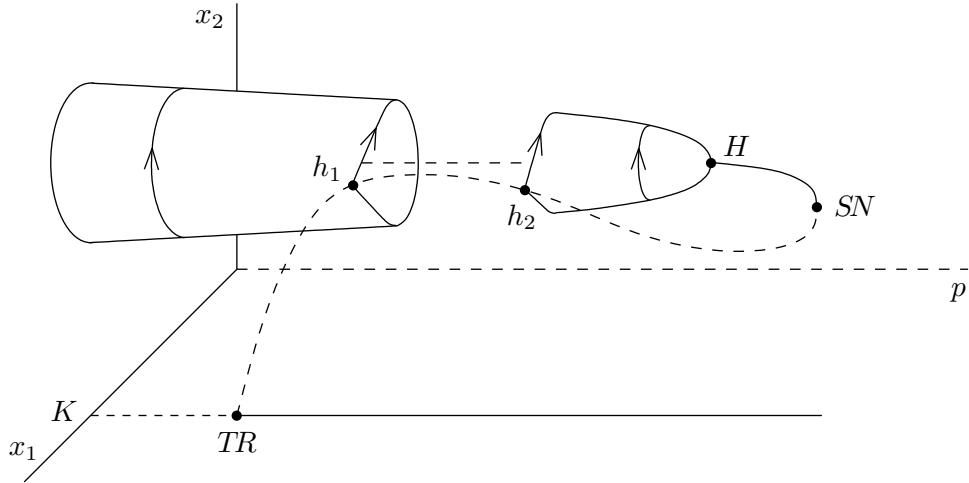


Figure 21: Equilibria and limit cycles (characteristic frame) of the Rosenzweig-MacArthur tritrophic food chain model with constant superpredator population p .

cycle (or, briefly, hysteresis). The catastrophes are therefore reversible, but after a transition from \mathcal{A}' to \mathcal{A}'' it is necessary to pass through a second catastrophe to come back to the attractor \mathcal{A}' . This simple type of hysteresis explains many phenomena in physics, chemistry, and electromechanics, but also in biology and social sciences. For example, the hysteresis of Figure 20B was used by Noy-Meir [1975] to explain the possible collapse (saddle-node bifurcation) of an exploited population described by the equation

$$\dot{x} = rx \left(1 - \frac{x}{K}\right) - \frac{ax}{1 + a\tau x} p,$$

where x is resource density (e.g., density of grass) and p is the number of exploiters (e.g., number of cows). If p is increased step by step (e.g., by adding one extra cow every year) the resource declines smoothly until it collapses to zero when a threshold p_2^* is passed. To regenerate the resource, one is obliged to radically reduce the number of exploiters to $p < p_1^*$.

Hysteresis can be more complex than in Figure 20 not only because the attractors involved in the hysteric cycle can be more than two, but also because some of them can be cycles. To show the latter possibility, we consider the so-called Rosenzweig-MacArthur model [Rosenzweig & MacArthur, 1963], that describes the dynamics of a tritrophic food chain (x_1 : prey; x_2 : predator; p : superpredator) in which, however, the top population is (or is kept) constant. Without entering into the details of the analysis of this second-order model [see Kuznetsov *et al.*, 1995], we show in Figure 21 the equilibria and the cycles of the system in the control space (p, x_1, x_2) for a specified value of all other parameters. The figure points out five

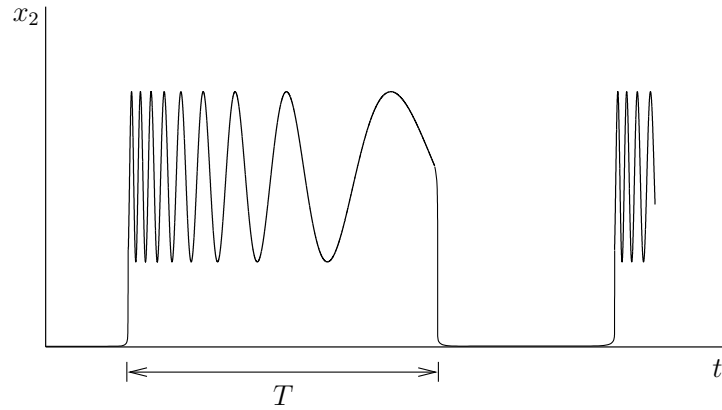


Figure 22: Periodic variation of a predator population induced by a periodic variation of the superpredator.

bifurcations: a transcritical (TR), two homoclinic (h_1 and h_2), a supercritical Hopf (H), and a saddle-node (SN). Two of these bifurcations, namely the second homoclinic h_2 and the saddle-node SN , are catastrophic and irreversible. In fact, catastrophic transitions from h_2 and SN bring the system toward the trivial equilibrium $(K, 0)$ (extinction of the predator population) and from this state it is not possible to return to h_2 or SN by varying p step by step. By contrast, the two other catastrophic bifurcations, namely the first homoclinic h_1 and the transcritical TR , are reversible and identify a hysteretic cycle obtained by varying back and forth the parameter p in an interval slightly larger than $[p_{TR}, p_{h_1}]$. On one extreme of the hysteresis we have a catastrophic transition from the equilibrium $(K, 0)$ to a prey-predator limit cycle. Then, increasing p , the period of the limit cycle increases (and tends to infinity as $p \rightarrow p_{h_1}$), and on the other extreme of the hysteresis we have a catastrophic transition from a homoclinic cycle (in practice a cycle of very long period) to the equilibrium $(K, 0)$. Thus, if p is varied smoothly, slowly, and periodically from just below p_{TR} to just above p_{h_1} , one can expect that the predator population varies periodically in time, as shown in Figure 22. In conclusion, the predator population remains very scarce for a long time and then suddenly regenerates, giving rise to high-frequency prey-predator oscillations which, however, slow down before a crash of the predator population occurs. Of course, tritrophic food chains do not always have such wild dynamics. In fact, many food chains are characterized by a unique attractor and therefore cannot experience catastrophic transitions and hysteresis.

An interesting variant of the hysteresis is the so-called *cusp*, described by the normal form

$$\dot{x} = p_1 + p_2x - x^3,$$

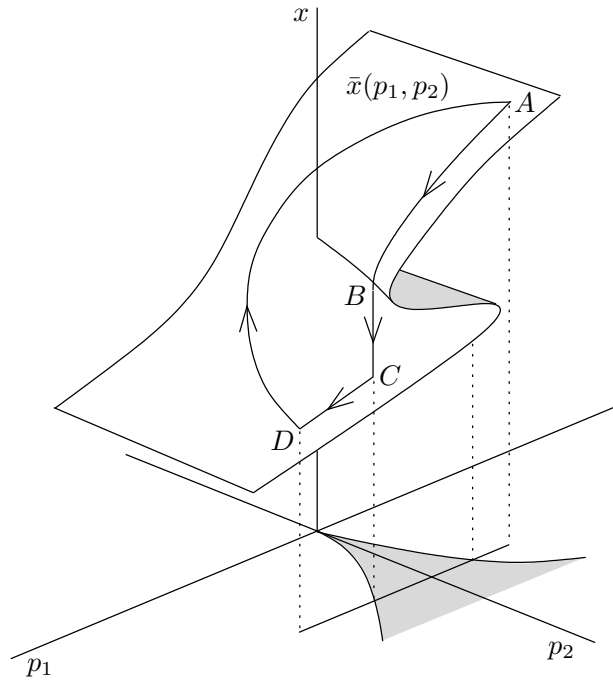


Figure 23: Equilibria of the cusp normal form. The unstable equilibria are on the gray part of the surface, which corresponds to the gray cusp region in the parameter space.

which is still a first-order system, but with two parameters. For $p_1 = 0$ the equation degenerates into the pitchfork normal form, while for $p_2 > 0$ the equation points out a hysteresis with respect to p_1 with two saddle-nodes. The graph of the equilibria $\bar{x}(p_1, p_2)$ is reported in Figure 23, which shows that for the parameters (p_1, p_2) belonging to the cusp region in parameter space, the system has three equilibria, two stable and one unstable (in the middle). In contrast with the hysteresis shown in Figure 20, this time after a catastrophic transition from an attractor \mathcal{A}' to an attractor \mathcal{A}'' (transition $B \rightarrow C$ in the figure), one can find the way to come back to \mathcal{A}' without suffering a second catastrophic transition (path $C \rightarrow D \rightarrow A \rightarrow B$ in the figure).

7 Routes to Chaos

The bifurcations we have seen in the previous sections deal with the most common transitions from stationary to cyclic regimes and from cyclic to quasi-periodic regimes. Only one of them, namely the homoclinic bifurcation in third-order systems, can mark, under suitable conditions specified by Shil'nikov theorem, the transition from a cyclic regime to a chaotic one. In an abstract sense, the Shil'nikov bifurcation is responsible of one of the most known “routes to chaos”, called *torus explosion*, characterized by the collision in

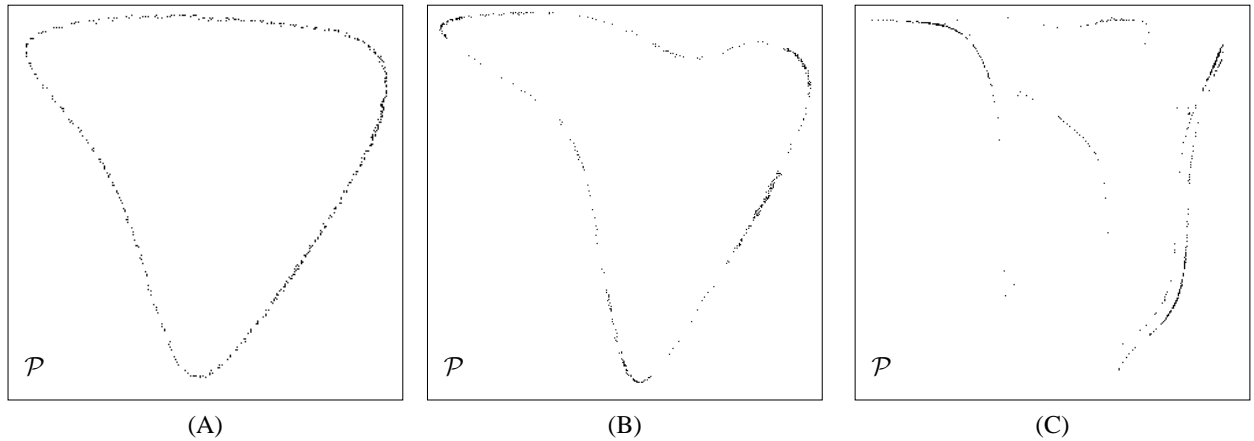


Figure 24: Torus explosion route to chaos viewed on a Poincaré section: (A) regular torus; (B) pinched torus; (C) strange attractor.

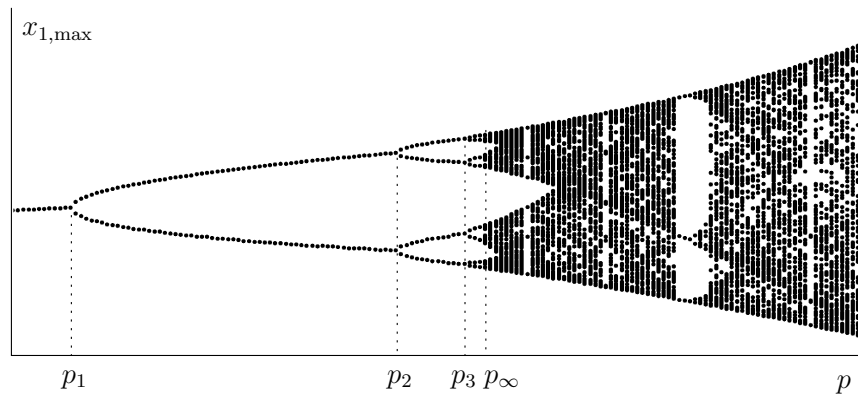


Figure 25: The Feigenbaum route to chaos: for $p \leq p_1$ the attractor is a cycle; for $p_1 < p < p_\infty$ the attractor is a longer and longer cycle; for $p \geq p_\infty$ the attractor is a strange attractor.

a three-dimensional state space of a saddle cycle with a stable torus. Observed on a Poincaré section, the bifurcation is revealed by a gradual change in shape of the intersection of the torus with the Poincaré section, shape which becomes more and more pinched while approaching the collision with the saddle cycle. After the collision, the torus breaks into a complex fractal set which, however, retains the geometry of a pinched closed curve, as shown in Figure 24.

Another, and perhaps most known, route to chaos is the *Feigenbaum cascade*, which is an infinite sequence $\{p_i\}$ of flip bifurcations where the p_i 's accumulate at a critical value p_∞ after which the attractor is a genuine strange attractor. Very often, this route to chaos is depicted by plotting the local peaks of a state variable, say x_1 , as a function of a parameter p , as shown in Figure 25. Physically speaking, the attractor remains a cycle until $p = p_\infty$, but the period of the cycle doubles at each bifurcation p_i , while unstable,

actually saddle, cycles of longer and longer periods accumulate in state space. This route to chaos points out a general property of strange attractors, namely the fact that they are basically composed by an aperiodic trajectory visiting a bounded region of the state space densely filled of saddle cycles, repelling along some directions (stretching) and attracting along others (folding).

8 Numerical Methods and Software Packages

All effective software packages for numerical bifurcation analysis are based on *continuation* (see, e.g., Keller, 1977, Allgower & Georg, 1990, Doedel *et al.*, 1991a,b, Beyn *et al.*, 2002, Kuznetsov, 2004, Chapter 10), which is a general method for producing in \mathbf{R}^q a curve defined by $(q - 1)$ equations

$$\begin{aligned} F_1(w_1, w_2, \dots, w_q) &= 0, \\ F_2(w_1, w_2, \dots, w_q) &= 0, \\ &\vdots \\ F_{q-1}(w_1, w_2, \dots, w_q) &= 0, \end{aligned}$$

or, in compact form,

$$F(w) = 0, \quad w \in \mathbf{R}^q, \quad F : \mathbf{R}^q \rightarrow \mathbf{R}^{q-1}. \quad (13)$$

Given a point $w^{(0)}$ that is approximately on the curve, i.e., $F(w^{(0)}) \simeq 0$, the curve is produced by generating a sequence of points $w^{(i)}$, $i = 1, 2, \dots$, that are approximately on the curve (i.e., $F(w^{(i)}) \simeq 0$), as shown in Figure 26A. The i th iteration step, from $w^{(i)}$ to $w^{(i+1)}$, is a so-called prediction-correction procedure with adaptive step-size and is illustrated in Figure 26B. The prediction $hw^{(i)}$ is taken along the direction tangent to the curve at $w^{(i)}$, where $v^{(i)}$ is computed as the vector of length 1 such that $\partial F / \partial w|_{w=w^{(i)}} v^{(i)} = 0$, the absolute value of h , called the step-size, is the prediction length, and the sign of h controls the direction of the continuation. Then, suitable corrections try to bring the predicted point back to the curve with the desired accuracy, thus determining $w^{(i+1)}$. If they fail, the step-size is reduced and the corrections are tried again until they succeed or the step-size goes below a minimum threshold at which the continuation halts with failure. By contrast, if corrections succeed at the first trial, the step-size is typically increased.

Given a second-order system $\dot{x} = f(x, p)$, where p is a single parameter, assume that an equilibrium

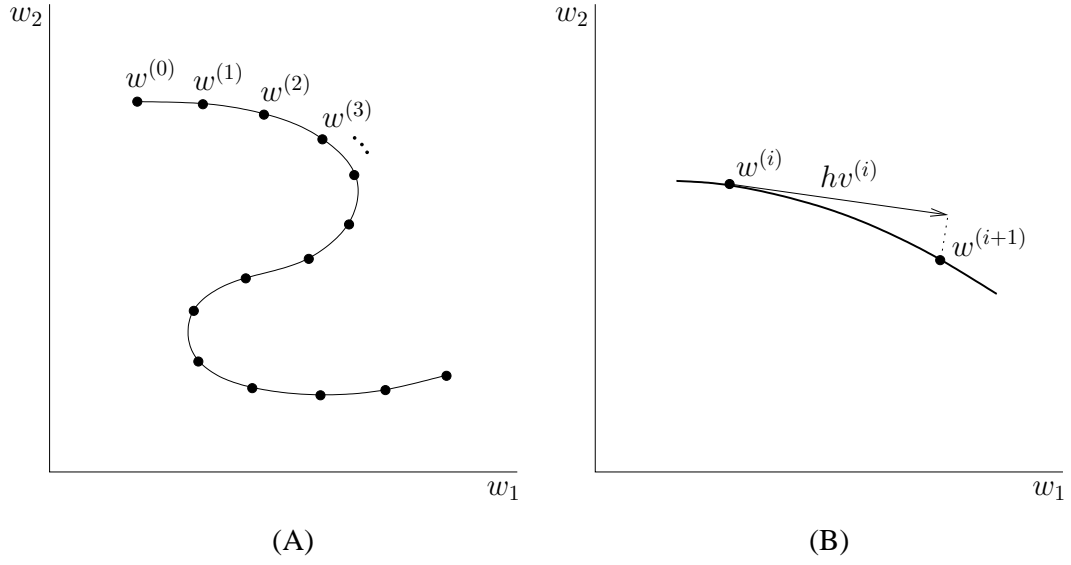


Figure 26: Generation of the curve defined by (13) through continuation.

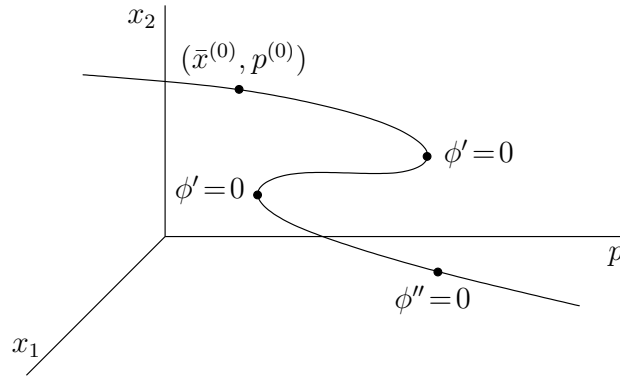


Figure 27: The curve $\bar{x}(p)$ produced from $(\bar{x}^{(0)}, p^{(0)})$ through continuation in the three-dimensional control space (p, x_1, x_2) and three bifurcation points, detected through the annihilation of the bifurcation functions ϕ' and ϕ'' .

$\bar{x}^{(0)}$ is known for $p = p^{(0)}$. Thus, starting from point $(\bar{x}^{(0)}, p^{(0)})$ in \mathbf{R}^3 , the equilibria $\bar{x}(p)$ can be easily produced, as shown in Figure 27, through continuation by considering (13) with

$$F(w) = f(x, p), \quad w = \begin{bmatrix} x \\ p \end{bmatrix}.$$

Moreover, at each step of the continuation, the Jacobian $J(\bar{x}(p), p)$ and its eigenvalues $\lambda_1(p)$ and $\lambda_2(p)$ are numerically estimated and a few indicators $\phi(\bar{x}(p), p)$, called *bifurcation functions*, are computed. These indicators annihilate at specific bifurcations, as shown in Figure 27. For example, $\phi' = \det(J)$ is a bifur-

cation function of transcritical, saddle-node, and pitchfork bifurcations, since at these bifurcations one of the eigenvalues of the Jacobian matrix is zero and $\det(J) = \lambda_1 \lambda_2$. Similarly, $\phi'' = \text{trace}(J)$ is a Hopf bifurcation function (see Section 4). Once a parameter value annihilating a bifurcation function has been found, a few simple tests are performed to check if the bifurcation is really present or to detect which is the true bifurcation within a set of potential ones. For example, as clearly pointed out by Figure 11B, at a saddle-node bifurcation the p -component of the vector tangent to the curve $\bar{x}(p)$ annihilates. By contrast, at transcritical and pitchfork bifurcations (see Figures 11A and C) two equilibrium curves, one of which is $\bar{x}(p)$, transversally cross each other, so that there are two tangent vectors at $p = p^*$, one with a vanishing p -component in the pitchfork case. Analogously, if $\phi''(\bar{x}(p^*), p^*) = 0$ one must first check that $\phi'(\bar{x}(p^*), p^*)$ is positive before concluding that $p = p^*$ is a Hopf bifurcation (see Section 4).

Once a particular bifurcation has been detected through the annihilation of its bifurcation function ϕ , it can be continued by activating a second parameter. For this, (13) is written with

$$F(w) = \begin{bmatrix} f(x, p) \\ \phi(x, p) \end{bmatrix}, \quad w = \begin{bmatrix} x \\ p \end{bmatrix},$$

where w is now four dimensional since p is a vector of two parameters. If the curve obtained through continuation in \mathbf{R}^4 is projected on the two-dimensional parameter space, the desired bifurcation curve is obtained.

In the case of local bifurcations of limit cycles and global bifurcations, the functions ϕ are quite complex and their evaluation requires the solution of the ODEs $\dot{x} = f(x, p)$. Actually, a rigorous treatment of the problem brings one naturally to the formulation of two-boundary-value problems [Doedel *et al.*, 1991b, Beyn *et al.*, 2002]. For example, as shown in Figure 28, homoclinic bifurcations can be detected by the function $\phi = z^+ - z^-$, where z^+ and z^- are the intersections of the unstable and stable manifolds of the saddle with an arbitrary axis z passing through the saddle. Thus, ϕ is zero if and only if the saddle has a homoclinic connection.

Many are the available software packages for bifurcation analysis, but the most interesting ones are AUTO [Doedel, 1981, Doedel *et al.*, 1997, 2007], LOCBIF [Khibnik *et al.*, 1993], CONTENT [Kuznetsov & Levitin, 1997], and MATCONT [Dhooge *et al.*, 2002]. They can all be used to study systems with more than two state variables and they can detect and continue all bifurcations mentioned in this chapter. AUTO is

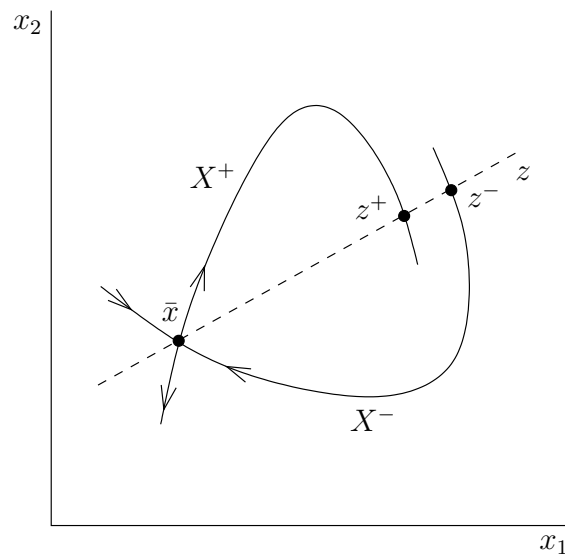


Figure 28: The bifurcation function $\phi = z^+ - z^-$ is zero when there is a homoclinic bifurcation, i.e., when the stable and unstable manifolds X^- and X^+ of the saddle collide.

the most popular software for bifurcation analysis and is particularly suited for the analysis of global bifurcations. LOCBIF is more effective than AUTO for local bifurcations, since it can also continue codimension-2 bifurcations. However, LOCBIF runs only on MS-DOS and has therefore been reimplemented and improved in CONTENT, which runs on several software platforms. MATCONT, continuously updated, is aimed at encapsulating the best features of all previously mentioned software packages in a MATLAB environment.

References

- Allgower, E. L. & Georg, K. (1990) *Numerical Continuation Methods: An Introduction*. Springer-Verlag, Berlin.
- Alligood, K. T., Sauer, T. D., & Yorke, J. A. (1996) *Chaos: An Introduction to Dynamical Systems*. Springer-Verlag, New York.
- Andronov, A. A., Leontovich, E. A., Gordon, I. J., & Maier, A. G. (1973) *Theory of Bifurcations of Dynamical Systems on a Plane*. Israel Program for Scientific Translations, Jerusalem.
- Beyn, W.-J., Champneys, A. R., Doedel, E. J., Govaerts, W., Kuznetsov, Yu. A., & Sandstede, B. (2002) Numerical continuation, and computation of normal forms. In *Handbook of Dynamical Systems*, ed. Fiedler, B., Elsevier Science, Burlington, MA, vol. 2, pp. 149–219.

- Dercole, F. & Rinaldi, S. (2008) *Analysis of Evolutionary Processes: The Adaptive Dynamics Approach and its Applications*. Princeton University Press, Princeton, NJ.
- Dhooge, A., Govaerts, W., & Kuznetsov, Yu. A. (2002) MATCONT: A MATLAB package for numerical bifurcation analysis of ODEs. *ACM T.Math. Software* **29**, 141–164.
- Doedel, E. J. (1981) AUTO, a program for the automatic bifurcation analysis of autonomous systems. *Cong. Numer.* **30**, 265–384.
- Doedel, E. J., Champneys, A. R., Dercole, F., Fairgrieve, T. F., Kuznetsov, Yu. A., Oldeman, B., Paffenroth, R. C., Sandstede, B., Wang, X. J., & Zhang, C. H. (2007) AUTO-07p: Continuation and bifurcation software for ordinary differential equations. Department of Computer Science, Concordia University, Montreal, QC.
- Doedel, E. J., Champneys, A. R., Fairgrieve, T. F., Kuznetsov, Yu. A., Sandstede, B., & Wang, X. J. (1997) AUTO97: Continuation and bifurcation software for ordinary differential equations. Department of Computer Science, Concordia University, Montreal, QC.
- Doedel, E. J., Keller, H. B., & Kernévez, J.-P. (1991a) Numerical analysis and control of bifurcation problems (I): Bifurcation in finite dimensions. *Int. J. Bifurcat. Chaos* **1**, 493–520.
- Doedel, E. J., Keller, H. B., & Kernévez, J.-P. (1991b) Numerical analysis and control of bifurcation problems (II): Bifurcation in infinite dimensions. *Int. J. Bifurcat. Chaos* **1**, 745–772.
- Guckenheimer, J. & Holmes, P. (1997) *Nonlinear Oscillations, Dynamical Systems and Bifurcations of Vector Fields*. Springer-Verlag, New York, 5th ed.
- Keller, H. B. (1977) Numerical solution of bifurcation and nonlinear eigenvalue problems. In *Applications of Bifurcation Theory*, ed. Rabinowitz, P. H., Academic Press, New York, pp. 359–384.
- Khibnik, A. I., Kuznetsov, Yu. A., Levitin, V. V., & Nikolaev, E. V. (1993) Continuation techniques and interactive software for bifurcation analysis of ODEs and iterated maps. *Physica D* **62**, 360–370.
- Kuznetsov, Yu. A. (2004) *Elements of Applied Bifurcation Theory*. Springer-Verlag, Berlin, 3rd ed.

- Kuznetsov, Yu. A. & Levitin, V. V. (1997) CONTENT: A multiplatform environment for analyzing dynamical systems. Dynamical Systems Laboratory, Centrum voor Wiskunde en Informatica, Amsterdam, The Netherlands (<ftp.cwi.nl/pub/CONTENT>).
- Kuznetsov, Yu. A., Muratori, S., & Rinaldi, S. (1995) Homoclinic bifurcations in slow-fast second-order systems. *Nonlinear Anal.* **25**, 747–762.
- Marsden, J. & McCracken, M. (1976) *Hopf Bifurcation and its Applications*. Springer-Verlag, New York.
- Noy-Meir, I. (1975) Stability of grazing systems: An application of predator-prey graphs. *J. Ecol.* **63**, 459–483.
- Rinaldi, S. (1993) The theory of complex systems. In *Biosystems and Complexity*, eds. Belardinelli, E. & Cerutti, S., Patron, Bologna, pp. 15–64 (in Italian).
- Rosenzweig, M. L. & MacArthur, R. H. (1963) Graphical representation and stability conditions of predator-prey interactions. *Am. Nat.* **97**, 209–223.
- Shil'nikov, L. P. (1968) On the generation of periodic motion from trajectories doubly asymptotic to an equilibrium state of saddle type. *Math. USSR-Sb* **6**, 427–437.
- Strogatz, S. H. (1994) *Nonlinear Dynamics and Chaos*. Addison-Wesley, Reading, MA.
- Thom, R. (1972) *Structural Stability and Morphogenesis*. Benjamin, Reading, MA (in French; English translation by Benjamin, 1975).